N93-25932

MULTI-RATE, REAL TIME IMAGE COMPRESSION FOR IMAGES DOMINATED BY POINT SOURCES

A. Kris Huber, Scott E. Budge, and Richard W. Harris
Department of Electrical Engineering
Utah State University
Logan, Utah 84322-4120

Abstract. An image compression system recently developed for compression of digital images dominated by point sources is presented. Encoding consists of minimum-mean removal, vector quantization, adaptive threshold truncation, and modified Huffman encoding. Simulations are presented showing that the peaks corresponding to point sources can be transmitted losslessly for low signal-to-noise ratios (SNR) and high point source densities while maintaining a reduced output bit rate. Encoding and decoding hardware has been built and tested which processes 552,960 12-bit pixels per second at compression rates of 10:1 and 4:1. Simulation results are presented for the 10:1 case only.

1. Introduction

Infrared images of space can be characterized by point sources such as stars and galaxies, spatially structured sources from galactic matter, moving objects such as planets and asteroids, and the background due to the zodiacal dust in the solar system [1]. We present a data compression algorithm tailored to this type of image when point sources and/or small moving objects are the primary features of interest.

The compression algorithm involves a combination of a the lossy algorithm, mean-residual vector quantization (MRVQ) [2,3,4], and the lossless algorithms run-length encoding and Huffman encoding [5,6]. While moderate-sized MRVQ encodes many scenes very well, including space backgrounds of low spatial frequency, MRVQ is not efficient for encoding point sources, since they are characterized by very high spatial frequencies. Thus the intent of the lossless stage is to encode the largest of the MRVQ errors and transmit as many of them as possible from the space platform using the telemetry bandwidth not needed by the MRVQ.

Section 2 discusses the compression algorithm. Section 3 describes the scene and instrument models used for the experiments of Section 4. Section 5 is a summary and conclusion.

2. A Multi-Rate Hybrid Algorithm

The descriptions of the algorithm given in this section includes some implementation details specific to the system built at the Space Dynamics Laboratory (SD) in Logan, Utah, for the Spirit 3 infrared radiometer. Some hardware trade-off issues for this algorithm are discussed in [7]. While hardware details are distinct from the algorithm itself, they may help the reader to visualize the encoding process. Refer to Figures 1 and 2 for a block diagram of the following encoding algorithm steps:

1) **Minimum-Mean Removal**. The mean background level is estimated and subtracted from the original image. The estimate is made by computing the sample means of four 16-pixel blocks (vectors) and choosing the minimum. The minimum mean is subtracted from all four vectors, resulting in the *mean residual*. The mean value is passed to the data multiplexor (Step 7) via a first-in first-out (FIFO) buffer, along with a small amount of side information which
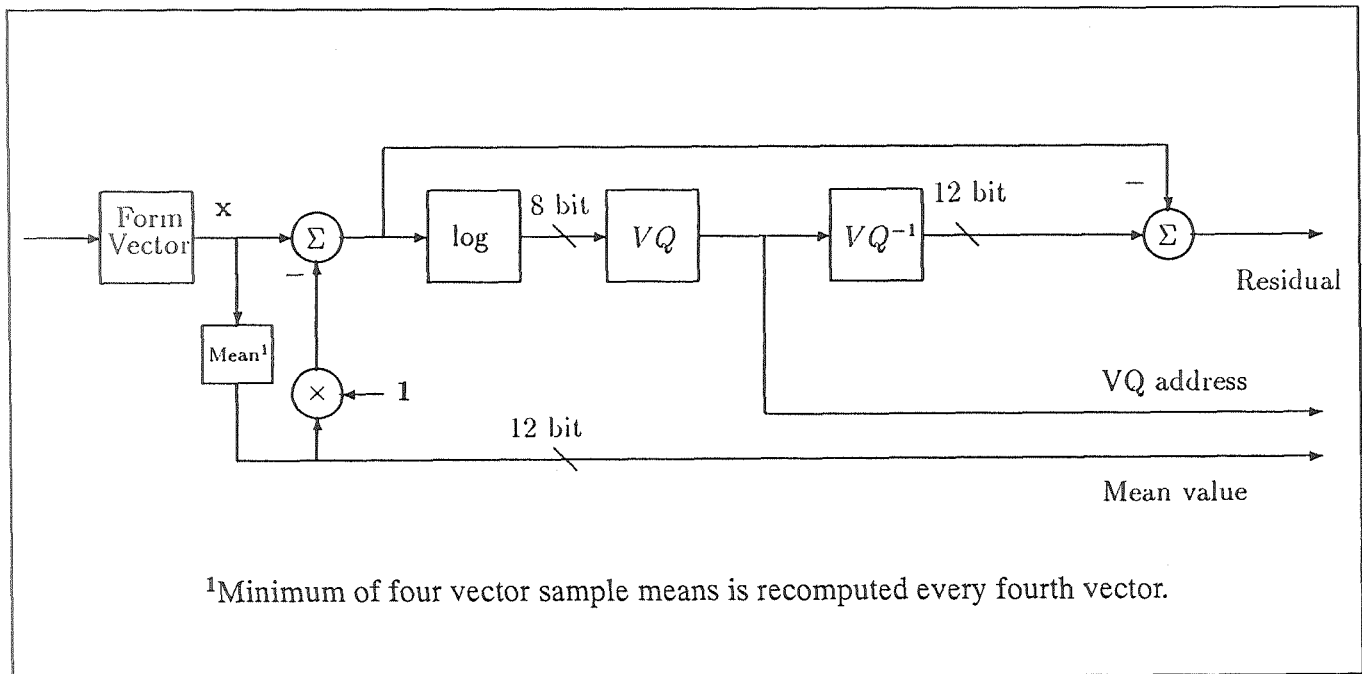
125

Figure 1. Block diagram of lossy encoding section, steps 1 through 3.
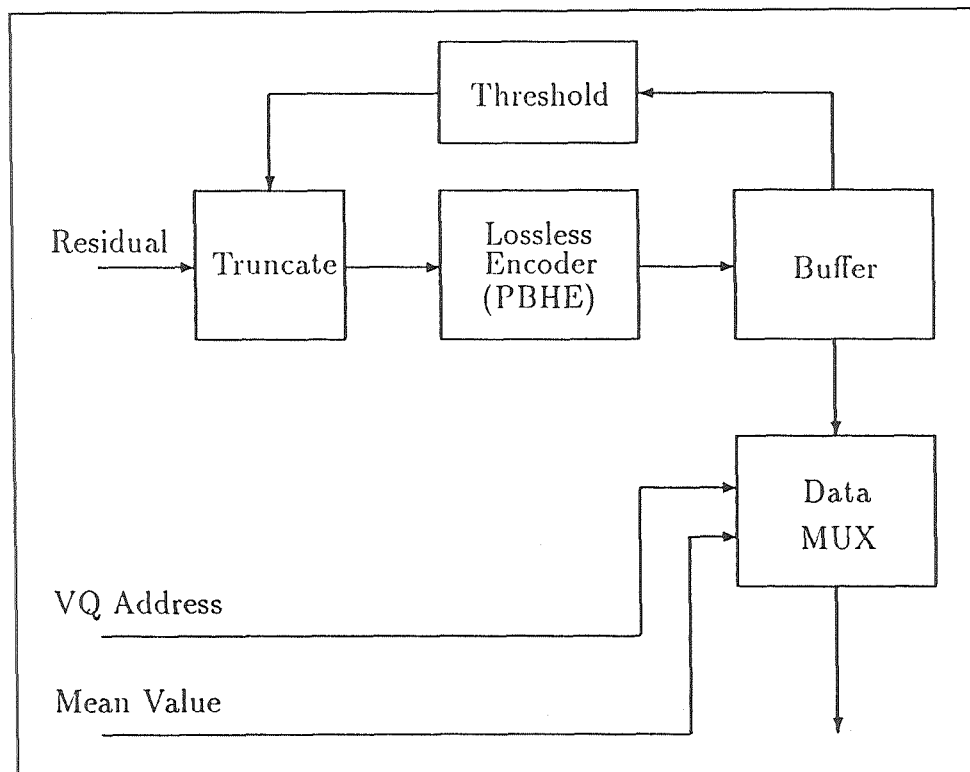

Figure 2. Block diagram of lossless stage, steps 4 through 7.

126

includes some key housekeeping words. From the side information the decoder determines whether the data is being compressed at a ratio of 4:1 or 10:1 and adjusts itself accordingly.

2) **Vector Quantization (VQ).** Each vector of *mean residual* is quantized to one of 256 codebook vectors. The codebook is structured as a 2-level tree with 16 vectors on the top level and 256 vectors on the bottom level. The codebook is searched real-time using a custom VLSI chip developed at Utah State University (USU) for VQ applications. The 13-bit mean residual pixels are converted to 9-bit values prior to VQ to accommodate the codebook processor chip. This is done by scaling the magnitude logarithmically using a look-up table. The magnitude of all values in the encoding codebook are also scaled in the same way (off-line). The address of the codebook vector with the least absolute difference from the residual vector is given to the data multiplexor (Step 7) via a FIFO buffer.

3) **Residual Formation.** The *residual* is the difference between the input vector and the MRVQ result. It is formed by an inverse VQ process and subtraction from the *mean residual*. The inverse VQ process involves accessing the decoding codebook memory to look up the 12-bit (magnitude not scaled) vector corresponding to the codebook vector chosen in Step 2.

4) **Adaptive Threshold Truncation.** The *residual* is compared pixel-by-pixel against a threshold which depends on the instantaneous fullness level of the buffer of lossless data (see Step 5). If the threshold is exceeded, the residual value is sent to the next encoding step, otherwise 0 is sent to the next step. The image formed by these values is called the *truncated residual*.

5) **Pixel-Based Huffman Encoding (PSYCHE).** The *truncated residual* is encoded losslessly by a combination of run-length and constrained Huffman coding. The codewords are precomputed off-line using an algorithm for constructing codewords of limited maximum length [6]. A special "header" codeword is reserved to prefix very large or very unlikely residual values. This reduces the amount of memory required to store the codewords. Encoding involves grouping the zeroes into runs and retrieving variable-length codewords from memory to represent runs and residual values. Codewords are packed end-to-end and placed in a FIFO buffer. The buffer is also accessed by the data multiplexor (Step 7), which empties it at a constant rate that depends on the selected compression ratio. The buffer fullness level is used to establish the adaptive threshold of Step 4.

6) **Synchronization and Error Detection.** At the end of each frame a synchronization codeword is transmitted, followed by a frame count. The synchronization codeword is such that it cannot be confused with any possible concatenations of codewords. The frame count is used by the decoder in the event of a loss of synchronization to correctly associate the lossless data frame with the MRVQ data frame. A 16-bit cyclic redundancy check (CRC) is inserted by the data multiplexor (Step 7). If the CRC computed by the decoder does not match, the lossless frame is not decoded. This feature prevents the large errors that would occur if a mis-aligned truncated residual were summed with the decoded MRVQ image.

7) **Data Multiplexing.** A predefined telemetry frame format is understood by both encoder and decoder. This format specifies the number of bits of mean, VQ, and lossless data sent in each telemetry frame. Mean values, VQ addresses and lossless data are drawn from their respective FIFO buffers according to the telemetry frame format and transmitted to Earth. The overall compression ratio is determined by the number of bits per frame into the compressor divided by the number of bits in the telemetry frame. Therefore adjustments can be made to the compression ratio by adjusting either the input data rate and/or the telemetry frame itself. Two modes are defined in the Spirit 3 compressor with compression ratios of 10:1 and 4:1. The difference between the two modes is that the 4:1 mode has a slower input rate and a telemetry frame with a higher proportion of lossless data. This multiple-rate capability is necessary or

desirable in many image compression systems, particularly for sensors which have the capability of sampling at various rates but transmit their data through a telemetry channel of fixed bandwidth.

8) **Establishment of Error Bounds.** Post processing can optionally be done to generate intervals that bound the true input signal. Whenever a non-zero residual value was transmitted losslessly the error is zero, thus the algorithm provides a subsampled image that is transmitted losslessly. Pixels where the residual was truncated by the adaptive threshold are in error by at most plus or minus the value of the threshold. Since the lossless buffer level can be determined by the delay between the MRVQ data and corresponding lossless data, the threshold can also be determined after encoding without sending side information if the threshold dependence on buffer level is known. In order to do this to full advantage, the hardware should be designed so that the signals which fill and empty the lossless FIFO are derived from the same clock, so they can be simulated exactly.

The decoding algorithm is simply the inverse of the encoding algorithm and will not be elaborated upon here.

3. Scene and Sensor Model

The hardware compression system is part of the Spirit 3 infrared radiometer built by the Space Dynamics Laboratory (SD) in Logan, Utah. This radiometer acquires data in five spectral bands from 2 to 26 microns in wavelength. An image is scanned across long rectangular focal plane arrays (FPAs) to form the scene. Some of the instrument parameters and performance estimates used in modelling the radiometer are given in Table 1. The data compressor provides quick-look capability to the instrument but is not the critical path for the data.

Table 1. Parameters used for simulating the SPIRIT 3 radiometer

NAME	Units	SPECTRAL BAND				
		A	B	C	D	E
Center Wavelength	μm	8.5	4.4	12	15	23
Bandwidth	μm	5	0.2	2.1	2.5	9.9
Integration Time	ms	2.8	2.8	2.8	2.8	2.8
Detector Field of View	sr	8.1E-09	8.1E-09	8.1E-09	8.1E-09	8.1E-09
Noise-Equivalent Radiance	W/cm^2-sr	3.1E-10	1.8E-09	2.2E-10	1.7E-10	1.8E-10

One of the missions of the instrument is to resolve natural and artificial point sources. To evaluate the performance of the algorithm under worst case conditions for point source scenes we used a scene generated by a state-of-the-art infrared scene generator, the Strategic Scene Generator Model (SSGM) version 2.3. In particular, we generated a scene of the galactic center where the point source density is the greatest. SSGM 2.3 documentation states that space scenes are subject to undercounting in the galactic plane, so the scene we generated is somewhere between the typical scene and the worst case.

In addition to the starfield and background, the sensor characteristics provide structure to the scene. In this system the data is delivered to the compressor uncalibrated, i.e. the measurements have not been corrected for the non-uniformity of response of the individual detectors in the array. Due to hardware constraints the image blocks are formed as 16x1 vectors with each pixel within a vector receiving data from the same spectral band, but from a different detector. Such non-

uniformity translates into higher entropy for the data stream and increases the importance of accurate sensor simulation when attempting to evaluate algorithm performance.

In our simulations we model the detector input, x, as

$$x = L * R_r + p_i * N * (L*R_r)^{0.5}$$

where L is the radiant flux value generated by the scene generator model (in $Wcm^{-2}sr^{-1}$), R_r is the nominal radiance responsivity (with units of counts per $Wcm^{-2}sr^{-1}$) that converts radiance to counts, N is a zero-mean unity-variance Gaussian random variable, and p_i is a detector coefficient to model the photon noise. Photon noise is a signal-dependent noise source that increases in direct proportion to the square root of the flux. Photon noise is caused by fluctuations in arrival rate of incident photons and ultimately limits the SNR [8].

We model the detector output as

$$f(x) = a_i + b_i x + c_i x^2 + N * d_i$$

where a_i, b_i and c_i are coefficients for offset, gain, and non-linearity that approximate the responsivity curve for each detector, and d_i is the standard deviation of the dark noise for each detector. The detector outputs are then uniformly quantized to obtain the 12-bit integer that is the input to the data compressor.

4. Experimental Results

Several experiments were performed to evaluate the performance of the algorithm. As noted in [9], average RMS error is statistically precise, but not always appropriate. In particular, large localized errors can occur with lossy compression techniques which do not increase the average error very much, but drastically diminish the quality of the compressed image by other standards. Therefore, in these simulations the distortion (in terms of RMS error) was tracked for pixels corresponding to point source peaks and reported separately from the distortion to pixels corresponding to background. All simulations were of the mode in which the compression ratio is 10:1 (1.2 bits per pixel).

Simulation #1 included preliminary estimates of focal plane coefficients. A 1 deg^2 infrared background scene for Simulation #1 was generated internally before the SSGM became available at SD.

For Simulations #2 and #3 the focal plane coefficients were based upon noise and responsivity tests performed by the focal plane vendors. Compared to the estimates of Simulation #1 the offset coefficients were less uniform, but the gain coefficients were more uniform. The infrared background scene generated by the SSGM was used for these simulations.

4.1 Simulation #1.

In this simulation the sensor coefficients were based on preliminary estimated values with the a_i, b_i, and c_i uniformly distributed over the intervals [10, 20], [0.8, 1.2], and $[-10^{-6}, 0]$, respectively. The dark noise, d_i, was modelled as uniform and equal to 1. The photon noise was also uniform across the detectors.

The detector non-uniformities effectively increased the noise sigma at the input to the data compressor from 1.0 to 5.5 counts. For this reason the point source SNR was referenced to the latter noise level. Point sources were positioned randomly and uniformly throughout the image. Their amplitude at the detector output divided by the noise sigma was considered to be the peak SNR of the point source.

Pre-processing consisted of generating an MRVQ codebook and PSYCHE codewords, which were shared by encoder and decoder. The residual codebook was generated using the LBG algorithm [4] from a training set consisting of the mean residual of a different background image. The PSYCHE codewords were based on codeword probabilities which were the average of probabilities estimated during preliminary runs of a different image with 12,000 and 24,000 point source pixels and SNR ranging from 5 to 30. The codeword lengths were computed using a modified form of the Huffman algorithm of Murakami, et. al. [6].

Root-mean-square (RMS) error in background pixels was nearly constant over the entire ensemble of simulation images as shown in Figure 3. Error in the point-source pixels is shown in Figure 4. No error occurred to point sources for SNR greater than 7 and number less than 24,000. Since the Spirit 3 radiometer scans a scene with four samples per dwell, and each point source is seen by all 8 FPA columns that are compressed, 24,000 point source pixels corresponds to a point source density of 750 per deg^2. For SNR less than 7, error in point source pixels and background pixels was comparable. As the number of point sources increased beyond 750 per deg^2, a substantial increase in error occurred which became higher with SNR (Figure 4). At such high densities PSYCHE was unable to encode all of the point source pixels with the allocated bandwidth. Those which were transmitted were still error-free.

4.2   Simulation #2.

In this simulation the sensor coefficients were based on roughly measured values (the data used to characterize the focal plane was not intended for calibration), but were probably closer to reality than in Simulation #1. The estimated means and standard deviations for the nominal detectors of the five focal plane arrays corresponding to the 5 spectral bands are given in Table 2. Where data was not available (indicated by n/a) a uniform focal plane was assumed (standard deviation of 0) and an average of available data was used for the mean.

Table 2.   Sensor Parameters for Simulation #2

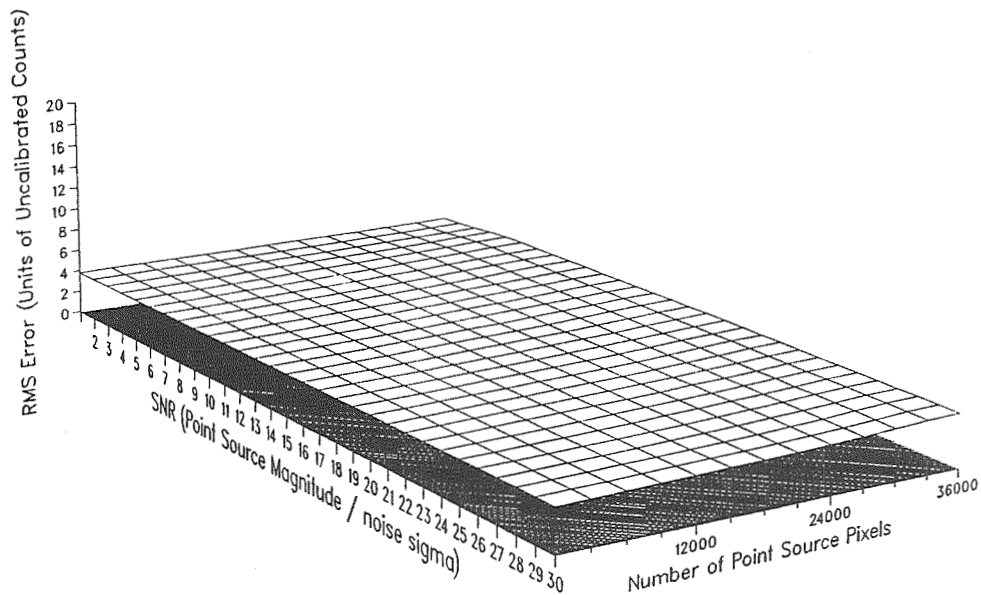| | | SPECTRAL BAND | | | | | |
		A	B	C	D	E	UNITS
a_i	Mean:	161	135	107	84	84	cnt
	Std:	39	n/a	19	23	17	cnt
b_i	Mean:	1.0	1.0	1.0	1.0	1.0	cnt/cnt
	Std:	n/a	n/a	.015	.020	.017	
c_i	Mean:	-10^{-5}	-10^{-5}	-10^{-5}	-10^{-5}	-10^{-5}	cnt/sqrt(cnt)
	Std:	n/a	n/a	n/a	n/a	n/a	
d_i	Mean:	0.6	0.6	0.9	0.9	0.9	cnt rms
	Std:	n/a	n/a	0.17	0.22	0.21	
p_i	Mean:	n/a	n/a	.128	.123	.122	cnt/sqrt(cnt)
	Std:	n/a	n/a	.009	.008	.008	

RMS Error to Background

Figure 3. Background error for varying SNR and number of sources, Simulation #1.
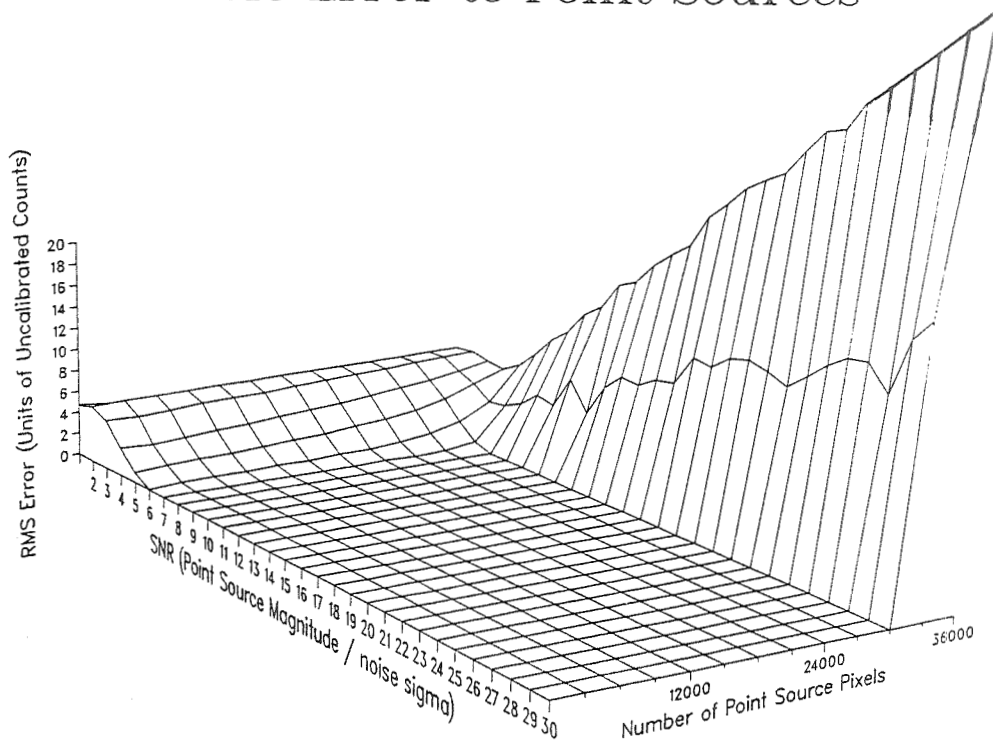
RMS Error to Point Sources

Figure 4. Point source error for varying SNR and number of sources, Simulation #1. 24,000 point source pixels corresponds to 750 sources per deg^2.

Separate images from the SSGM were used to train the compressor from those used to obtain performance results. As in Simulation #1, additional point sources of constant SNR were positioned randomly to evaluate how algorithm performance varied with point source density. Figure 5 shows the RMS error due to compression as a function of point source SNR and number density. These indicate that most of the point source radiance peaks are encoded losslessly for SNR above about 60 and point source density below about 300 per $\deg^2$. We believe the reason the average error in this region is non-zero is due to the few bad detectors in the focal plane arrays. The compression error to the background remained nearly constant at 4.6 counts until point source density became very high.

Note that in this simulation and the next, the definition of SNR was changed. The SNR was defined as the peak point source radiance in counts divided by the RMS dark noise, d_i. In other words we used the detector SNR and did not include the pseudo-noise at the compressor input due to non-uniformity as we did in Simulation #1.

Figure 6 shows the result when the simulation was repeated for a more ideal case. The dark noise was made equal for all spectral bands to 1 count rms, and the focal planes were assumed to be perfectly uniform (coefficients were set to the mean value for the nominal detectors). A significant improvement resulted. The point source peak radiance was encoded losslessly for SNR above about 8 and point source density below about 1000 per $\deg^2$. The background was encoded with RMS error of about 0.9 counts in this region.

4.3 Simulation #3.

In this simulation the sensor coefficients were the same as in Simulation #2. The original SSGM scene of the galactic center was compressed with and without non-uniformities. As an add-hoc method of compensating for the point source undercounting in our version of SSGM, we doubled the radiance of the SSGM scene. This gave a point source density of about 188 per $\deg^2$ for sources with an SNR of 3 and greater.

Figure 7 shows the RMS error to point sources when FPA non-uniformity was included. In this case point source peaks were transmitted losslessly for sources of SNR greater than 36. Background error was 4.5 counts rms.

Figure 8 shows the RMS error to point sources for the same scene imaged with uniform detector arrays and dark noise of 1 count rms. This caused the threshold above which point source peaks were transmitted losslessly to be reduced to 7. Background error in this case was reduced to 0.84 counts rms.

5. Summary and Conclusion

A hybrid lossy/lossless algorithm for compression of space images dominated by point sources was described. State of the art simulation software was used to model the infrared sky for the spectral bands of the radiometer. The model used to simulate some of the dominant sensor characteristics was described. The data derived from these models fed several data compression experiments in which the images were segmented into pixels corresponding to point sources and pixels corresponding to background. Errors caused by the compression algorithm operating at a compression ration of 10:1 were tracked separately for point sources and background.

The simulations showed that background was encoded quite well, but that focal plane uniformity could significantly reduce the errors due to the compression algorithm. A conclusion that can be drawn from this is that it is desirable to compress calibrated data when this is feasible.
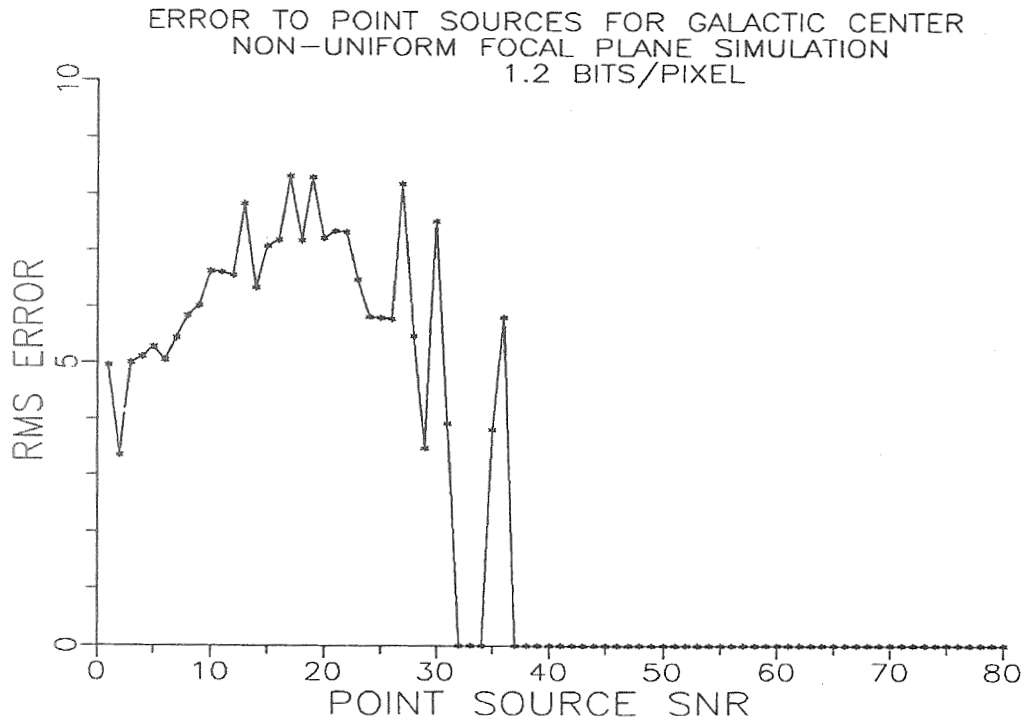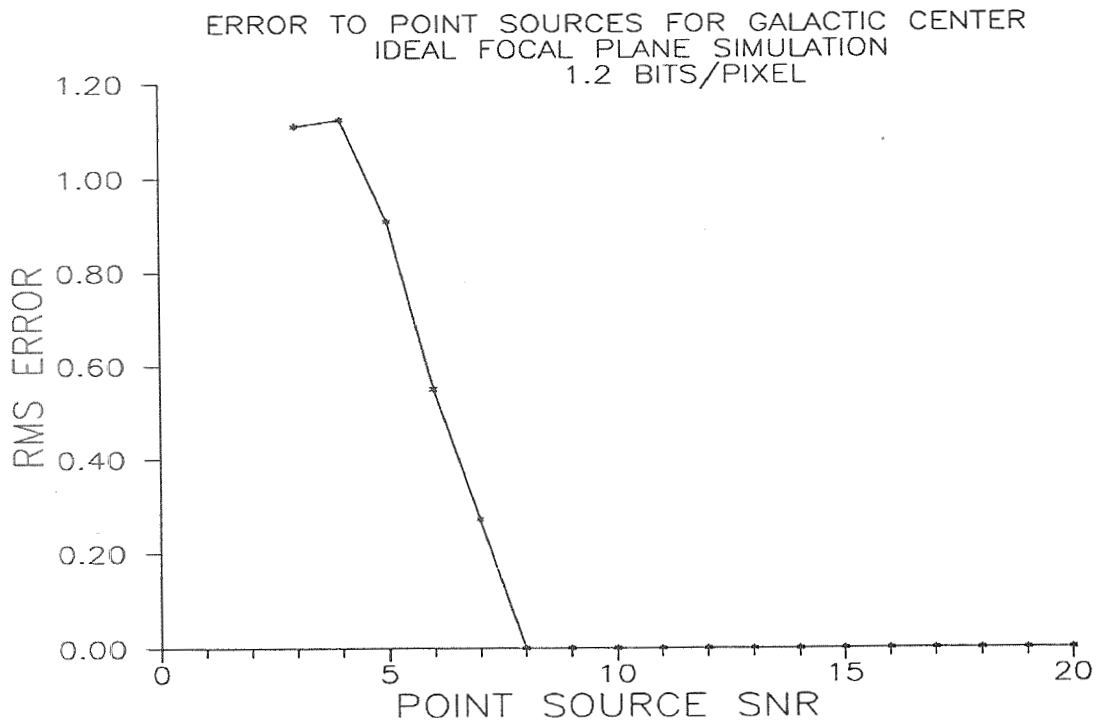
RMS Error to Point Sources
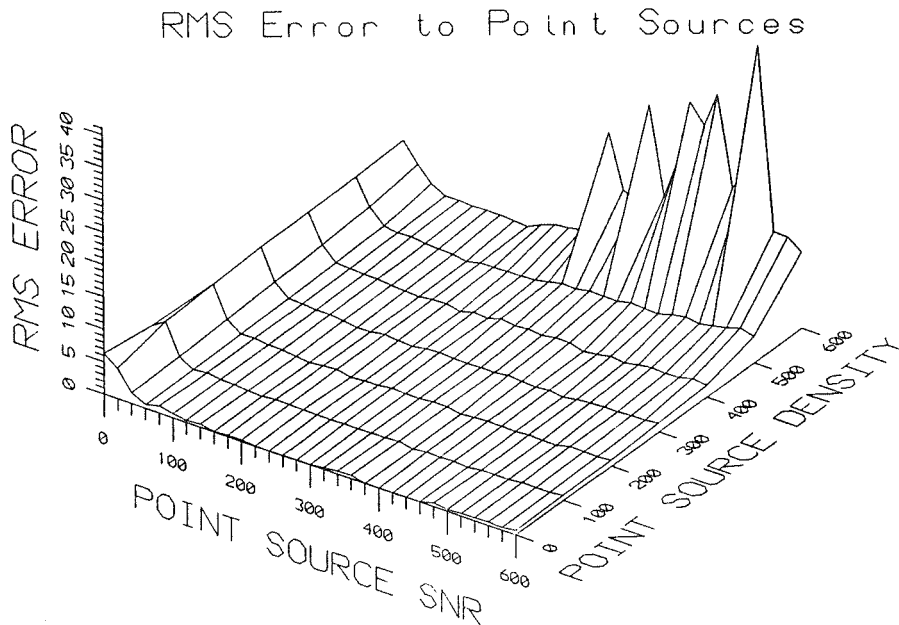
Figure 5. Simulation #2. RMS error (in counts) to point source peak values due to 10:1 compression. SNR was defined as the point source peak magnitude divided by the focal plane array dark noise coefficients. Non-uniformity of FPAs was simulated based on measured data. Background error was nearly constant at about 4.6 counts.

RMS Error to Point Sources
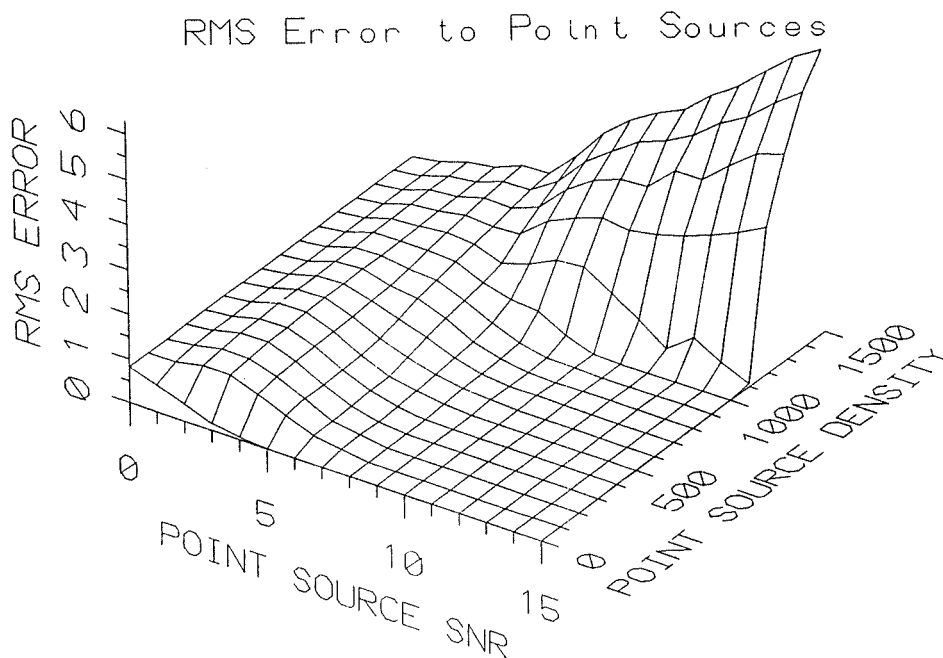
Figure 6. Simulation #2. RMS error (in counts) to point source peak values due to 10:1 compression. SNR was defined as the point source peak magnitude divided by the focal plane array dark noise. The mean offset and gain coefficients were used for all detectors of an array, thus simulating perfect uniformity. The background error was nearly constant at about 0.9 counts for the region plotted.

ERROR TO POINT SOURCES FOR GALACTIC CENTER
NON–UNIFORM FOCAL PLANE SIMULATION
1.2 BITS/PIXEL

RMS ERROR

POINT SOURCE SNR

Figure 7. Simulation #3. RMS error to point sources in the galactic scene imaged onto non-uniform focal plane arrays. Background error was 4.5 counts rms.

ERROR TO POINT SOURCES FOR GALACTIC CENTER
IDEAL FOCAL PLANE SIMULATION
1.2 BITS/PIXEL

RMS ERROR

POINT SOURCE SNR

Figure 8. Simulation #3. RMS error to point sources in the galactic scene imaged onto perfectly uniform focal plane arrays. Background error was 0.84 counts rms.

The simulations also showed that no error occurred to peaks of point sources over a wide range of point source densities and relatively low SNR. The trends of the graphs generated in Simulations #1 and #2 held in Simulation #3, namely low average error to background and lossless transmission of point source peaks detected with sufficient SNR. Excellent performance in that simulation indicates that the compressor should perform well when the sensor is sampling scenes that are dominated by point sources, such as those simulated. Reduction of simulated performance is expected due to optical blurring which was not simulated. Blurring will reduce the point source peak SNR and effectively increase the point source density.

Further research is needed to investigate the bounded error property of this algorithm and design enhancements and new algorithms that use this property to increase coding efficiency. Additionally, scientific algorithms for data reduction that use the time-varying compression error bound could be designed.

Acknowledgment

References

[1] Price, S. D. and Kenneally, J. P., "The Infrared Celestial Background Scene Descriptor," *Imaging Infrared: Scene Simulation, Modeling, and Real Image Tracking*. A. J. Huber, M. Triplett, J. Wolverton, Editors, Proc. SPIE 1110, pp. 38-48, 1989.

[2] Baker, R. L., "Vector Quantization of Digital Images," Ph.D. Dissertation, Stanford Univ., 1984.

[3] Gray, R. M., "Vector Quantization," *IEEE ASSP Magazine*, pp. 4-29, Apr. 1984.

[4] Linde, Y., Buzo, A., and Gray, R. M., "An Algorithm for Vector Quantizer Design," *IEEE Trans. Commun.*, vol. COM-28, pp. 84-95, Jan. 1980.

[5] Huffman, D. A., "A Method for the Construction of Minimum-Redundancy Codes," *Proc. IRE*, vol. 40, pp. 1098-1101, Sept. 1952.

[6] Murakami, H., Matsumoto, S., and Yamamoto, H., "Algorithm for Construction of Variable Length Code with Limited Maximum Word Length," *IEEE Trans. Commun.*, vol. COM-32, pp. 1157-1159, Oct. 1984.

[7] Singer, J. H., "System Implementation Trade-Offs of Lossless Data Compression Algorithms for Space Sensor Image Compression," M.S. Thesis, Utah State Univ., 1991.

[8] Wyatt, C. L., *Electro-Optical System Design for Information Processing*, McGraw-Hill: New York, 1991.

[9] Erickson, D. E., "Data Compression for Near Earth and Deep Space to Earth Transmission," *Space and Earth Science Data Compression Workshop*. J. C. Tilton, Editor, NASA Conference Publication 3130, Nov. 1991.